computation

MDPI

Article

Magnetohydrodynamic Blood-Carbon Nanotube Flow and Heat Transfer Control via Carbon Nanotube Geometry and Nanofluid Properties for Hyperthermia Treatment

Nickolas D. Polychronopoulos [1,*], Evangelos Karvelas [2], Lefteris Benos [3], Thanasis D. Papathanasiou [4] and Ioannis Sarris [1,*]

[1] Department of Mechanical Engineering, University of West Attica, Egaleo, 12241 Athens, Greece
[2] Department of Biomedical Engineering, University of West Attica, Egaleo, 12243 Athens, Greece; ekarvellas@uniwa.gr
[3] Institute of Bio-Economy and Agri-Technology (IBO), Centre of Research and Technology-Hellas (CERTH), 57001 Thessaloniki, Greece; e.benos@certh.gr
[4] Department of Mechanical Engineering, University of Thessaly, 38334 Volos, Greece; athpapathan@uth.gr
* Correspondence: nickpolys@gmail.com (N.D.P.); sarris@uniwa.gr (I.S.)

Abstract: Hyperthermia is a promising medical treatment that uses controlled heat to target and destroy cancer cells while minimizing damage to the surrounding healthy tissue. Unlike conventional methods, it offers reduced risks of infection and shorter recovery periods. This study focuses on the integration of carbon nanotubes (CNTs) within the blood to enable precise heat transfer to tumors. The central idea is that by adjusting the concentration, shape, and size of CNTs, as well as the strength of an external magnetic field, heat transfer can be controlled for targeted treatment. A theoretical model is developed to analyze laminar natural convection within a simplified rectangular porous enclosure resembling a tumor, considering the composition of blood, and the geometric characteristics of CNTs, including the interfacial nanolayer thickness. Using an asymptotic expansion method, ordinary differential equations for mass, momentum, and energy balances are derived and solved. Results show that increasing CNT concentration decelerates fluid flow and reduces heat transfer efficiency, while elongated CNTs and thicker nanolayers enhance conduction over convection, to the detriment of heat transfer. Finally, increased tissue permeability—characteristic of cancerous tumors—significantly impacts heat transfer. In conclusion, although the model simplifies real tumor geometries and treatment conditions, it provides valuable theoretical insights into hyperthermia and nanofluid applications for cancer therapy.

Keywords: targeted cancer therapy; porous tumor; natural convection; magnetohydrodynamic effect; blood-CNT thermal conductivity; asymptotic solutions

check for updates

Academic Editor: Sergey A. Karabasov

Received: 24 January 2025
Revised: 18 February 2025
Accepted: 20 February 2025
Published: 3 March 2025

Citation: Polychronopoulos, N.D.; Karvelas, E.; Benos, L.; Papathanasiou, T.D.; Sarris, I. Magnetohydrodynamic Blood-Carbon Nanotube Flow and Heat Transfer Control via Carbon Nanotube Geometry and Nanofluid Properties for Hyperthermia Treatment. *Computation* **2025**, *13*, 62. https://doi.org/10.3390/computation13030062

Copyright: © 2025 by the authors. Licensee MDPI, Basel, Switzerland. This article is an open access article distributed under the terms and conditions of the Creative Commons Attribution (CC BY) license (https://creativecommons.org/licenses/by/4.0/).

1. Introduction

Cancer remains one of the deadliest diseases worldwide, with an estimated 9.6 million deaths attributed to the disease in 2018 [1]. There are several types of cancer, including lung cancer [2], breast cancer [3], and cancer related to brain, such as glioblastoma multiforme [4]. The last one stands out as one of the most aggressive and challenging to treat cancers [5]. Cancer is generally characterized by invasive growth and resistance to conventional therapies [6]. Traditional treatments such as surgery, chemotherapy, radiotherapy, and immunotherapy offer some respite, but there are several limitations, including invasiveness, risks of necrosis, and resistance in certain tumors. Moreover, severe side effects,

such as an increased risk of infection, anemia, infertility, and nerve damage worsen the patient's health condition [7,8]. These drawbacks emphasize the urgent need for innovative and targeted therapies, that are both effective and minimally invasive.

Hyperthermia has emerged as a promising alternative for cancer treatment. The primary objective for the treatment is to elevate the tumor's temperature beyond the normal physiological range, thereby damaging the cancerous cells through various mechanisms like protein denaturation, apoptosis, and necrosis [9], while leaving the surrounding healthy tissue largely unaffected. Additionally, hyperthermia can also be employed alongside therapies such as chemotherapy and radiation to enhance their effectiveness by increasing the susceptibility of cancer cells to these treatments. While chemotherapy and radiation often lead to considerable adverse effects due to their non-selective impact on both malignant and healthy tissues, hyperthermia offers a localized and controlled therapeutic approach, thereby minimizing systemic side effects [10]. This characteristic positions hyperthermia as a promising alternative to traditional cancer treatments, enabling a more targeted, personalized, and less harmful therapeutic strategy [11]. In mild hyperthermia, the tumor temperature typically falls within the range of 40–45 °C, whereas for ablation therapy it may exceed 50 °C [12–14]. Despite its ancient origins, which can be traced back to Hippocrates [15], the modern resurgence of hyperthermia leverages advancements in heat transfer technologies and materials science, particularly nanotechnology, to overcome the limitations of conventional thermal therapies [16].

Recently, gold nanorods and CNTs have gathered significant attention for their role in targeted hyperthermia [17,18]. CNTs in particular exhibit extraordinary thermal and optical properties, and excel in absorbing electromagnetic energy for rapid heating [18,19] due to their quasi-one-dimensional (high aspect ratio) molecular structure [20,21]. The most frequent CNTs forms are single-walled carbon nanotubes (SWCNTs) and multi-walled carbon nanotubes (MWCNTs). In contrast with iron oxide nanoparticles, CNTs do not rely on absorbing energy from external magnetic fields for heat generation. Instead, they efficiently absorb energy from sources like near-infrared (NIR) radiation, enabling precise and localized heating [18,19]. Interestingly, CNTs also exhibit excellent heat conductivity and, therefore, may be considered as ideal candidates for heat transfer in hyperthermia [18]. There are several experimental studies on the use of CNTs for hyperthermia cancer treatment. Indicatively, Markovic et al. [22] employed CNTs and graphene-based nanoparticles to induce hyperthermia and eliminate human glioblastoma multiforme cells in vitro. Their study revealed that CNTs induced cancer cell death through mitochondrial membrane depolarization. In addition, Raniszewski et al. [23] employed CNTs with ferromagnetic nanoparticles to study the effect of the electromagnetic field in temperature distribution in human liver. Finally, Radzi et al. [24], studied the effects of MWCNTs combined with hyperthermia as a treatment for breast cancer on tumor-bearing mice. The results showed that mice treated with both MWCNTs and localized hyperthermia achieved complete tumor destruction, exhibiting at the same time a significant increase in median survival.

Modeling hyperthermia in tumors plays a crucial role for the efficient design of the treatment. Specifically, identifying the temperature distribution and gathering the information regarding the flow in the cancerous region are key factors that should be considered for treatment control and enhancement [16]. From the modeling perspective, tumors are frequently considered as a porous medium [25]. The porosity or permeability depends on several factors, including the type of the tumor and the stage of the tumor growth. To describe the flow and heat transfer within the porous tumor, the effective physical properties of the bio-nanofluid (blood and CNTs) can be taken into consideration. This is straightforward, for in the case of a nanofluid where the base fluid is a simple fluid, like water, eventually the mixture can be regarded as a single-phased nanofluid [26,27].

However, when the base fluid is blood, defining the effective properties is challenging due to the complex composition of blood: plasma, red and white blood cells, and platelets, at different percentages [28]. Few studies have addressed these complexities. For example, Benos et al. [16] developed a theoretical model for the description of the magnetohydrodynamic (MHD) blood-Fe_3O_4 flow and heat transfer in a simplified porous tumor geometry. In [29], a new theoretical model for the effective thermal conductivity of blood-CNT nanoparticles was developed. The model took into consideration several CNT design parameters, such as their size and shape and the blood composition. Their results indicated that the bio-nanofluid conductivity was greatly affected by the CNT geometry and the volume fraction of the CNTs, suggesting possible ways to regulate heat transfer during the hyperthermia treatment of glioblastoma multiforme by using CNTs.

While the blood-CNTs effective thermal conductivity model by Benos et al. [29] was developed in the context of hyperthermia for tumors, its application to the fundamental understanding of how the geometrical parameters of the CNTs control the flow and heat distribution in the tumor has not yet been carried out. In the present study, a theoretical MHD framework, based on the analysis from earlier works of our group [16,26,27], is developed, and asymptotic solutions are derived for both velocity and temperature fields. The MHD effect on the bio-nanofluid flow in the porous cancerous region serves to control the heat transfer and flow, similar to techniques like the Czochralski (CZ) crystal growth method for assuring better-quality crystals [30]. Finally, internal heating is utilized in this analysis to model the tumor heating, resulting from the interaction between CNTs and external energy sources. The insights from this analysis will improve our understanding of bio-nanofluid dynamics in hyperthermia, and pave the way for the experimental validation and clinical application of targeted thermal therapies using CNTs.

2. Materials and Methods

2.1. Flow Configuration and Boundary Conditions

In the present analysis, the porous tumor is assumed to have the geometry of a two-dimensional horizontal rectangular porous enclosure with a large aspect ratio (l/h), as illustrated in Figure 1. It is further assumed that the tumorous region is fully saturated with the bio-nanofluid, consisting of blood and CNTs. The boundary conditions are also shown in Figure 1; the vertical walls are isothermal, and the horizontal walls are adiabatic, while all walls are electrically insulated. The bio-nanofluid motion is driven by a volumetric internal heat source Q, while a uniform external magnetic field $\vec{B_0}$ is also applied in the vertical z-direction. Joule heating and viscous dissipation are assumed to be negligible, and the Boussinesq approximation is applied to account for the buoyancy force in Equation (3). The low magnetic Reynolds number (low-R_m) approximation is used in the magnetic induction equation, as the induced magnetic field is considered to be insignificant in comparison to the external magnetic field [31].

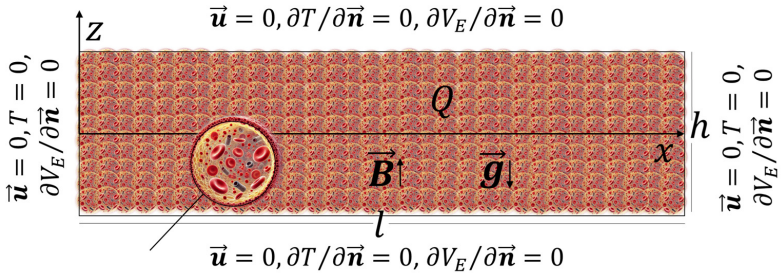


Figure 1. Flow configuration and boundary conditions. Vertical and horizontal walls are electrically insulated (V_E is the electrical potential). Vertical walls are isothermal and horizontal walls are adiabatic.

The governing equations that describe the MHD flow and heat transfer of the system are the following:

$$\frac{\partial u}{\partial x} + \frac{\partial w}{\partial z} = 0, \tag{1}$$

$$u\frac{\partial u}{\partial x} + w\frac{\partial u}{\partial z} = -\frac{1}{\rho_{bio}}\frac{\partial P}{\partial x} + v_{bio}\left(\frac{\partial^2 u}{\partial x^2} + \frac{\partial^2 u}{\partial z^2}\right) - \frac{\sigma_{bio}{B_o}^2 u}{\rho_{bio}} - \frac{v_{bio}}{K}u, \tag{2}$$

$$u\frac{\partial w}{\partial x} + w\frac{\partial w}{\partial z} = -\frac{1}{\rho_{bio}}\frac{\partial P}{\partial z} + v_{bio}\left(\frac{\partial^2 w}{\partial x^2} + \frac{\partial^2 w}{\partial z^2}\right) + \beta_{bio} g\Delta T - \frac{v_{bio}}{K}w, \tag{3}$$

$$u\frac{\partial T}{\partial x} + w\frac{\partial T}{\partial z} = a_{bio}\left(\frac{\partial^2 T}{\partial x^2} + \frac{\partial^2 T}{\partial z^2}\right) + \frac{Q}{\left(\rho C_p\right)_{bio}}. \tag{4}$$

In the above equations, "*bio*" terms correspond to the bio-nanofluid, u and w are the velocities in the x and z Cartesian coordinates, respectively, P is the pressure, g is the gravitational acceleration, ΔT is the temperature difference across the medium (in the z-direction), ρ is the density, C_p is the specific heat capacity, v is the kinematic viscosity ($v = \mu/\rho$, with μ the dynamic viscosity), σ is the electrical conductivity, β is the volumetric expansion coefficient, K is the permeability and $a_{bio} = k_{bio}/\left(\rho C_p\right)_{bio}$ is the thermal diffusivity of the bio-nanofluid. It should be mentioned that in Equation (2), the associated Lorentz force is expressed via the $\sigma_{bio}{B_o}^2 u$ term, as explained in detail in Benos et al. [31].

2.2. Estimation of Effective Properties

2.2.1. Thermal Conductivity

The effective thermal conductivity for the blood-CNTs nanofluid k_{bio}, in the present study is expressed by the following equation [29]:

$$k_{bio} = k_{plasma-CNT}\frac{k_{BC} + 2k_{plasma-CNT} + 2\left(k_{BC} - k_{plasma-CNT}\right)\varphi_{BC}}{k_{BC} + 2k_{plasma-CNT} - \left(k_{BC} - k_{plasma-CNT}\right)\varphi_{BC}}, \tag{5}$$

where $k_{plasma-CNT}$ is given by:

$$k_{plasma-CNT} = k_{plasma}\frac{k_{pe} + k_{plasma}(n-1) + (n-1)\left(k_{pe} - k_{plasma}\right)\varphi_e}{k_{pe} + k_{plasma}(n-1) - \left(k_{pe} - k_{plasma}\right)\varphi_e}, \tag{6}$$

and k_{BC} is the thermal conductivity of the blood cells, φ_{BC} is the volume fraction of the blood cells, k_{plasma} is the thermal conductivity of plasma, k_{pe} is the thermal conductivity of the equivalent nanoparticle, given by the following expression:

$$k_{pe} = k_l\frac{2k_{CNT} + \left[\left(1 + \frac{t}{b}\right)^2 - 1\right](k_{CNT} + k_l)}{2k_l + \left[\left(1 + \frac{t}{b}\right)^2 - 1\right](k_{CNT} + k_l)}, \tag{7}$$

φ_e is the equivalent nanoparticle volume fraction expressed via:

$$\varphi_e = \left(1 + \frac{t}{b}\right)^2\varphi, \tag{8}$$

with k_l being the thermal conductivity of the interfacial nanolayer given by:

$$k_l = k_{plasma}\frac{1 + \frac{t}{b} - a}{a\frac{t}{b}}\frac{\ln\left(1 + \frac{t}{b}\right)}{\ln\left(\frac{1+\frac{t}{b}}{a}\right)}, \tag{9}$$

with t being the thickness of the nanolayer. In Equation (9) the a parameter corresponds to the half-length of the CNT ($S = 2a$) and the parameter b is the radius of the CNT or in terms of the diameter, $d = 2b$. Also, the n parameter in Equation (6) is obtained from:

$$n = sph^{-\gamma}, \tag{10}$$

where the sphericity sph is given by:

$$sph = \frac{2e(\delta)\left[1 - e^2(\delta)\right]^{1/6}}{e(\delta)\sqrt{1 - e^2(\delta)} + \arcsin[e(\delta)]}, \tag{11}$$

where e stands for the eccentricity of the nanoparticle and δ ranges between 0 and t [32]. Note that for elongated particles (γ power in Equation (10)), Jiang et al. [32] obtained $\gamma = 1.55$ for CNTs. The dependence of k_{bio} on the above-described geometrical parameters and volume fraction is presented in Figure 2a–e.

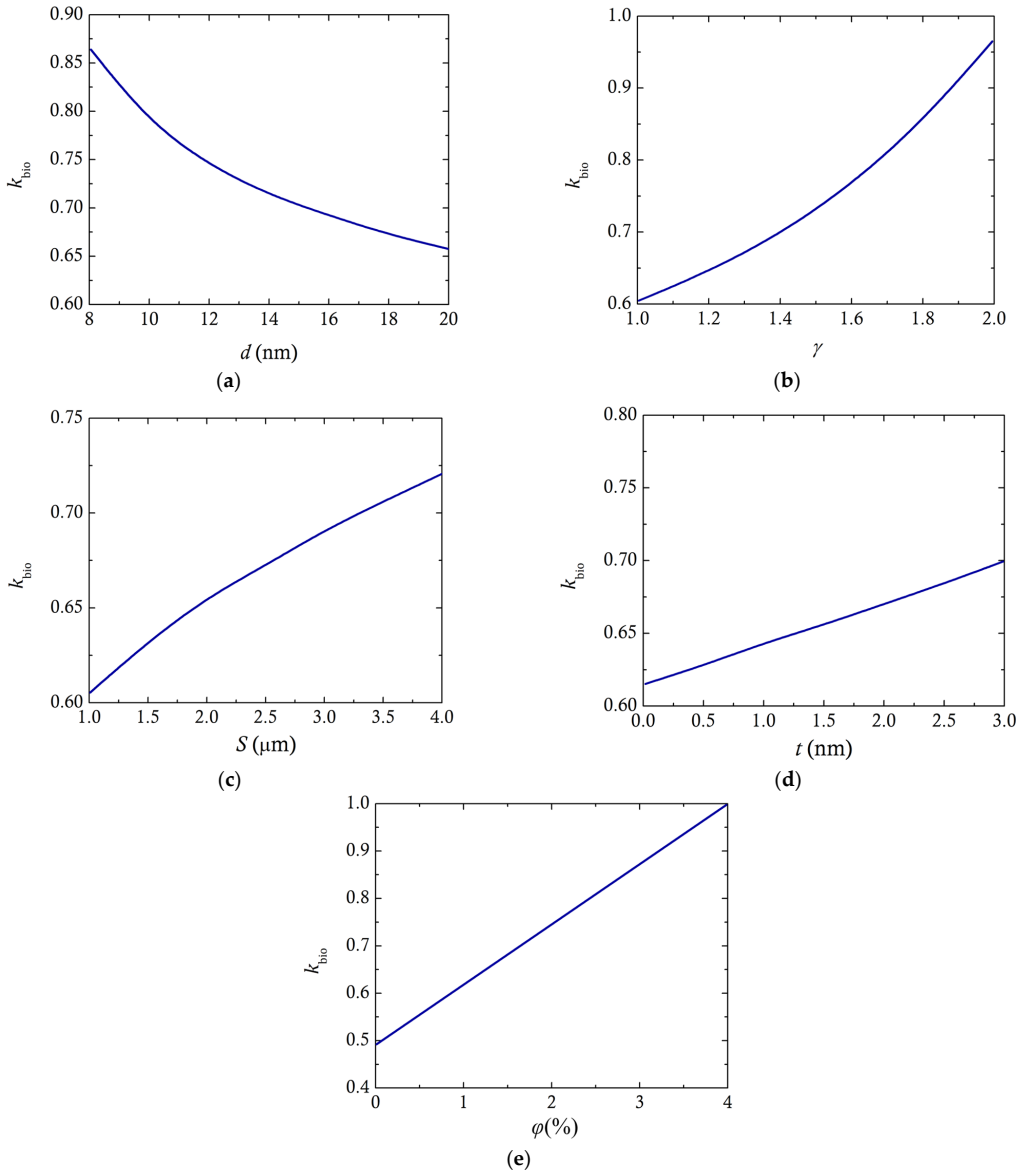


Figure 2. Effect of the different CNT geometrical factors and volume fraction on k_{bio}: (**a**) diameter, d, (**b**) γ parameter, (**c**) length, S, (**d**) nanolayer thickness, t, and (**e**) volume fraction, φ.

In short, as the diameter of the CNTs increases, the effective thermal conductivity, k_{bio}, decreases. In contrast, increasing γ, CNT length, nanolayer thickness, and the concentration of CNTs results in higher values of k_{bio}.

2.2.2. Dynamic Viscosity

From a general perspective, blood viscosity is a property that characterizes blood resistance while flowing through the vessels and soft tissues. Due to its non-Newtonian nature, blood exhibits a viscosity that varies based on multiple physiological and pathological factors, including plasma viscosity, erythrocyte deformability, hematocrit levels, and the balance of erythrocyte aggregation and disaggregation, among others. Notably, these properties can be significantly altered by various disease states, emphasizing the clinical relevance of understanding blood rheology [33]. However, when the shear rate exceeds 100 s^{-1}, blood behavior can be approximated as Newtonian [34]. To simplify the current analysis, only plasma (the largest portion of blood [29]), that is the Newtonian component of blood, will be modeled, with its viscosity assumed to have an average value of 1.25 cP (1.25 mPa·s) [29]. Employing the Brinkman model, a model frequently utilized in contemporary biomedical studies [35,36], the effective dynamic viscosity of the bio-nanofluid can be expressed as:

$$\mu_{bio} = \mu_{pl} \frac{1}{(1-\varphi)^{2.5}}, \tag{12}$$

where μ_{pl} is the blood plasma viscosity.

2.2.3. Rest of Effective Properties

Following the earlier studies [26,36], the rest of the effective properties can be calculated from the equations shown below:

$$\rho_{bio} = (1-\varphi)\rho_{pl} + \varphi\rho_{\mathrm{CNT}}, \tag{13}$$

$$(\rho C_p)_{bio} = (1-\varphi)(\rho C_p)_{pl} + \varphi(\rho C_p)_{CNT}, \tag{14}$$

$$(\rho\beta)_{bio} = (1-\varphi)(\rho\beta)_{bio} + \varphi(\rho\beta)_{CNT}, \tag{15}$$

$$\sigma_{bio} = \sigma_{bio}\left[1 + \frac{3\varphi\left(\frac{\sigma_{CNT}}{\sigma_{pl}} - 1\right)}{\left(\frac{\sigma_{CNT}}{\sigma_{pl}} + 2\right) - \varphi\left(\frac{\sigma_{CNT}}{\sigma_{pl}} - 1\right)}\right], \tag{16}$$

where the subscript "*pl*" refers to blood plasma. Finally, the thermophysical properties of blood plasma and SWCNT, according to the relevant literature [37–39], are summarized in Table 1.

Table 1. Thermophysical properties of blood plasma and SWCNT [37–39].

Property	Symbol	Blood Plasma	SWCNT
Density	ρ (Kgm^{-3})	1030	2600
Specific heat under constant pressure	C_p ($JKg^{-1}K^{-1}$)	3930	425
Thermal conductivity	k ($Wm^{-1}K^{-1}$)	0.57	6600
Volumetric expansion coefficient	β (K^{-1})	1×10^{-4}	1.6×10^{-6}
Dynamic viscosity	μ (Pas)	1.25×10^{-3}	-
Electrical conductivity	σ (Sm^{-1})	0.05	4.8×10^{7}

2.3. Dimensionless Equations with Analytical Solutions

Following the asymptotic analysis of Benos et al. [27], by the use of the streamfunction ψ, the flow and energy equations along with the boundary conditions result in the following form:

$$\nabla^4\psi = \mathrm{Pr}_{bio}^{-1}\frac{\partial(\nabla^2\psi,\psi)}{\partial(x,z)} + \left({Ha_{bio}}^2 + Da^{-1}\right)\nabla^2\psi + \mathrm{Ra_{bio}}\frac{\partial\theta}{\partial x}, \tag{17}$$

$$\nabla^2\theta + 1 = \frac{\partial(\theta,\psi)}{\partial(x,z)}, \tag{18}$$

$$\psi = \frac{\partial\psi}{\partial x} = \theta = 0\ (at\ x = 0, L),\ \psi = \frac{\partial\psi}{\partial z} = \frac{\partial\theta}{\partial z} = 0\ (at\ z = -0.5,\ 0.5), \tag{19a}$$

$$\psi(x,\,z) = -\psi(L - x,\,z),\ \theta(x,\,z) = \theta(L - x,\,z), \tag{19b}$$

where the following dimensionless numbers are introduced, namely the Prandtl number:

$$Pr_{bio} = \frac{v_{bio}}{a_{bio}}, \tag{20}$$

the Darcy number:

$$Da = \frac{K}{h^2}, \tag{21}$$

the Rayleigh number:

$$Ra_{bio} = \frac{g\beta_{bio}Qh^5}{\left(\rho C_p\right)_{bio}v_{bio}a_{bio}^2}, \tag{22}$$

and the Hartmann number:

$$Ha_{bio} = B_o h(\sigma_{bio}/\rho_{bio}v_{bio})^{1/2}, \tag{23}$$

When deriving the above equations, the following magnitudes were considered [16]: $\widetilde{x} = \frac{x}{h}, \widetilde{z} = \frac{z}{h}, \widetilde{\psi} = \frac{\psi}{a_{bio}}, \widetilde{\theta} = \frac{T\left(\rho c_p\right)_{bio}a_{bio}}{h^2Q}$ and the circumflex "~" was omitted for convenience.

The above dimensionless numbers are widely used in fluid mechanics and heat transfer to express the ratio of momentum to thermal diffusivity (Pr), the ratio of the relative strength of electromagnetic to viscous forces (Ha), and the relative effect of the permeability versus the medium cross-sectional area (Da). Finally, by definition, Ra is the ratio of gravitational forces to thermal diffusion.

For pure conduction, the temperature at $z = 0$ can be given through $\theta = \frac{1}{2}x(L - x)$ [40]. Finally, by introducing $\xi = x/L, z = z$, the scaled Ra is given by:

$$Rs_{bio} = Ra_{bio}{\cdot}L. \tag{24}$$

Benos et al. [27] derived the following solutions for streamfunction (ψ_o), vertical velocity (w_o) and temperature in the core region (θ_o):

$$\psi_0 = -2\ \frac{{a_m}^{-1/2}\,G}{{Ha_{bio}}^2 + Da^{-1}}\sinh\frac{1}{3}y_m, \tag{25}$$

$$w_0 = -\frac{\partial\psi_0}{\partial\xi} = \frac{Rs_{bio}\,G}{\left({Ha_{bio}}^2 + Da^{-1}\right)\left(1 + 4\,sinh^2\frac{1}{3}y_m\right)}, \tag{26}$$

$$\theta_0 = a_m^{-1}\,Rs_{bio}^{-2}\left(cosh\frac{2}{3}y_m - \frac{1}{2}cosh\frac{4}{3}y_m - cosh\frac{2}{3}y_{m,0} + \frac{1}{2}cosh\frac{4}{3}y_{m,0}\right). \tag{27}$$

In the above Equations (20)–(22), the variables G, y_m, $y_{m,0}$ and a_m are given by:

$$G(z) = \frac{1}{2}\left(\frac{cosh\left(\sqrt{{Ha_{bio}}^2 + Da^{-1}}z\right)}{\sqrt{{Ha_{bio}}^2 + Da^{-1}}sinh\left(\frac{\sqrt{{Ha_{bio}}^2+Da^{-1}}}{2}\right)} - \frac{coth\left(\sqrt{{Ha_{bio}}^2 + Da^{-1}}/2\right)}{\sqrt{{Ha_{bio}}^2 + Da^{-1}}} + \frac{1}{4} - z^2 \right), \quad (28)$$

$$y_m = sinh^{-1}\left[\frac{3}{2}{a_m}^{1/2}Rs_{bio}\left(\xi - \frac{1}{2}\right)\right], \quad (29)$$

$$y_{m,0} = sinh^{-1}\left(\frac{3}{4}{a_m}^{1/2}Rs_{nf}\right), \quad (30)$$

$$\alpha_m = \frac{3}{(Ha_{bio} + Da)^2}\int_{-0.5}^{0.5} G\left(z\right)^2 dz\,. \quad (31)$$

For the further investigation of the heat transfer in the tumorous region, the ratio of heat transfer by convection to the corresponding one by conduction was considered, expressed by Nusselt number, Nu. Specifically, similarly to the relevant literature [31,40], the average Nusselt number was utilized, given by:

$$Nu_{av} = \frac{1}{T(0.5L,\ 0.5)}\int_{-0.5}^{0.5}\frac{\partial T}{\partial x}(0,z)dz = \frac{L}{2T(0.5L,\ 0.5)} \approx \frac{1}{2L\theta_0(0.5)}\,. \quad (32)$$

The comprehensive analysis detailing the derivation of the asymptotic solutions is presented in the Appendix of [27].

3. Results

In this section, we present the results regarding the dimensionless temperature and vertical velocity distribution along the scaled ξ coordinate (or in dimensional terms the x-coordinate) as well as results for the streamfunction ψ, average Nusselt number $Nu_{av.}$, and Da number. Consistent with [16,27,31], our analysis concentrates on the core region where the asymptotic solutions remain valid, as proved in [31] via validation against computational results for the same flow setup and boundary conditions. The above results are exhibited in terms of the geometrical properties of the CNTs, with the aim to provide a fundamental understanding on how the CNT geometry can control the MHD flow and heat transfer in the porous tumor. Towards that direction, we have assumed some reference values for our setting and carried out a parametric study with respect to the CNTs geometry effect. The reference values are the following: $Rs_{bio} = 5000$, $Ha_{bio} = 5$, $Da = 0.02$, $\varphi = 2\%$, $d = 12$ nm, $t = 1.5$ nm, $\gamma = 1.55$ and $L = 2$ μm.

The effect of CNTs diameter, d, on MHD flow and heat transfer of the bio-nanofluid is shown in Figure 3. In particular, Figure 3a exhibits the dimensionless temperature $\theta_o(\xi)$ profile with its maximum being at the tumor center. For this case, only the d parameter varies, and the reference values of the rest of the parameters are held constant. The top red dotted line corresponds to the case of pure conduction in the porous tumor and presents the limiting case. Increasing the diameter of the CNTs leads to a decrease in the dimensionless temperature in the tumor.

This results in enhancing the heat transfer in the tumor by convection, which is exhibited by the increase in the streamfunction ψ_o values in Figure 3b in the core region, as well as an increase in the vertical velocity w_o (Figure 3c). This can be explained from the relation of the effective thermal conductivity to the CNT diameter (Figure 2a). Increasing d leads to a substantial decrease in the thermal conductivity of the bio-nanofluid. In turn, from the definition of the Rayleigh number in Equation (22), Ra_{bio} increases, leading to the convective heat transfer becoming the dominant heat transfer mode. The above behavior

is also evident in Figure 3d where the value of Nu_{av} increases from approximately 0.84 to 0.96, corresponding to a 14.29% increase as d increases from 8 nm to 20 nm.

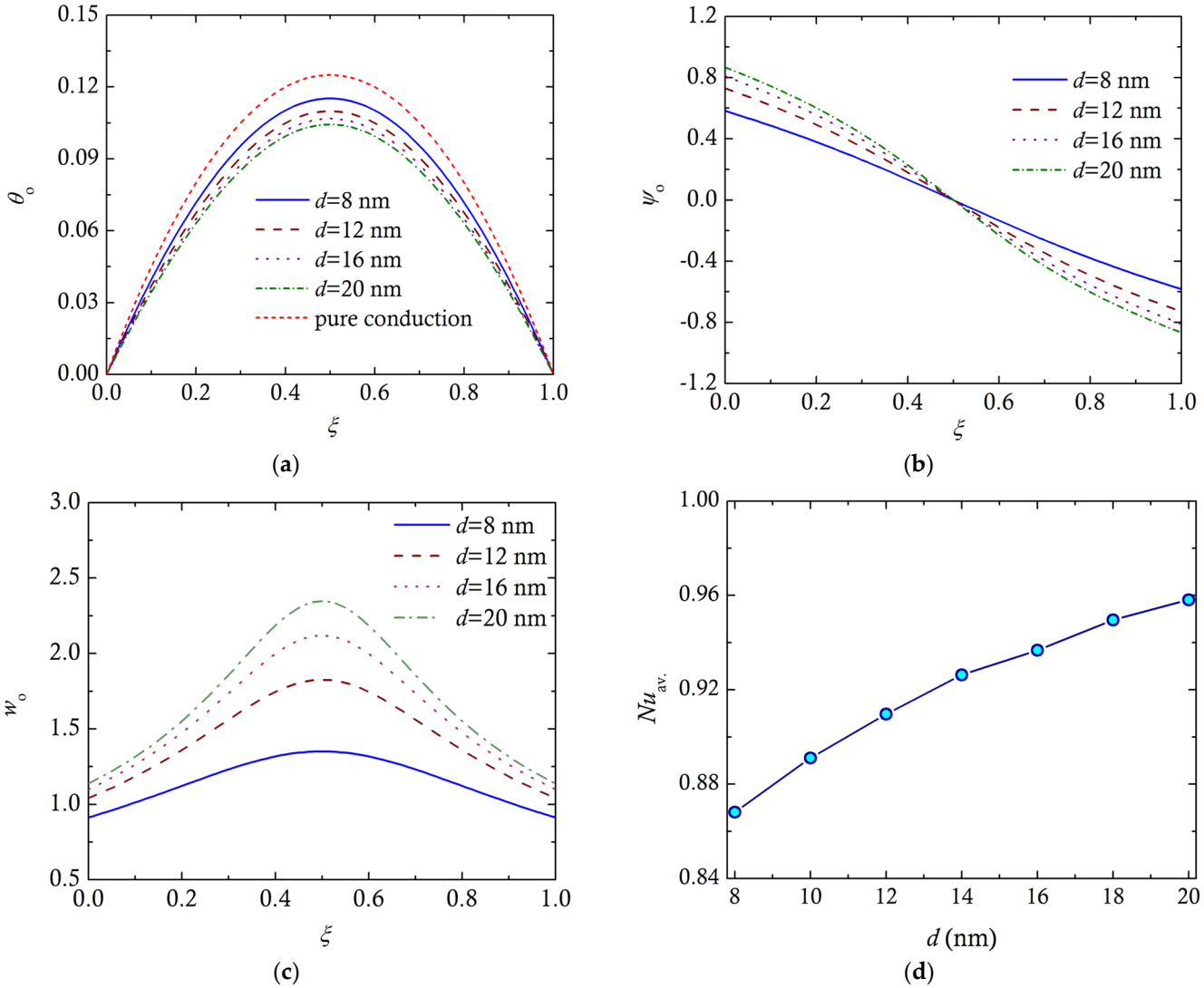


Figure 3. Results for different CNT diameter values, d: (**a**) dimensionless temperature profile, $\theta_{0.}$, (**b**) streamfunction, ψ_0, (**c**) dimensionless vertical velocity, w_o, and (**d**) average Nusselt number $Nu_{av.}$.

The effect of the γ parameter is shown in Figure 4 (the values of the rest of the parameters are kept constant). As the γ parameter increases, the dependence of n on sph (see Equation (10)) is stronger and the effective thermal conductivity of the bio-nanofluid increases, as shown in Figure 2b, leading to a decrease in Rs_{bio}. This is expected to decrease the convective heat transfer. The above behavior, with regard to the temperature profile in the core region, is depicted in Figure 4a. Specifically, the temperature increases, and for very elongated CNT nanoparticles (larger values of γ) the temperature distribution is close to that of pure conduction. In turn, this is accompanied by a deceleration of the bio-nanofluid motion in the porous enclosure, which is exhibited by the decrease in both the streamfunction values and the vertical velocity in the core region, shown in Figures 4b and 4c, respectively. Figure 4d shows that by increasing γ, Nu_{av} decreases in an almost linear manner.

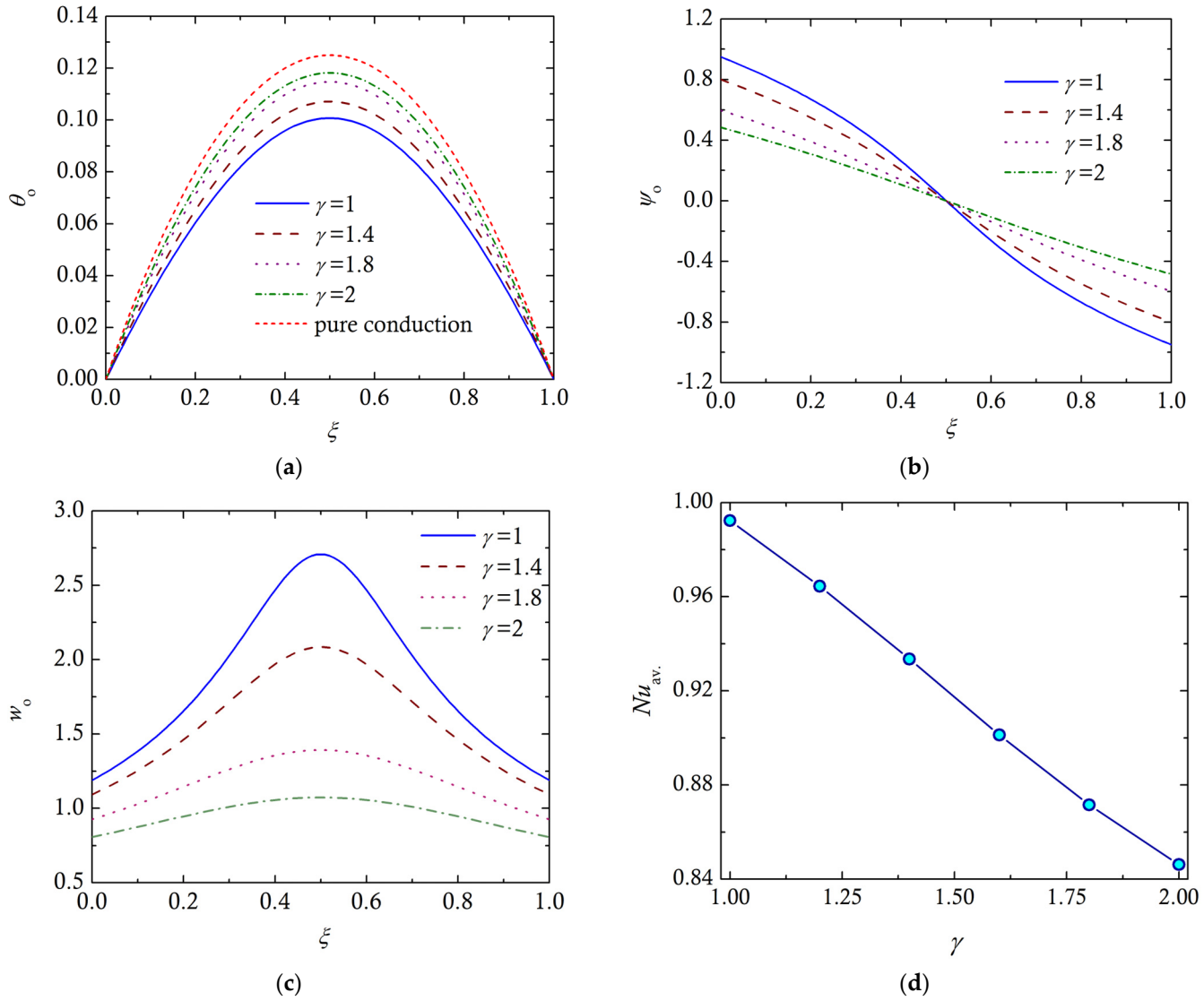


Figure 4. Results for different γ values in the core region: (**a**) dimensionless temperature profile, $\theta_{0.}$, (**b**) streamfunction, ψ_0, (**c**) dimensionless vertical velocity, w_o, and (**d**) average Nusselt number $Nu_{av.}$.

The effect of the CNTs length, S, on the MHD flow and heat transfer of the bio-nanofluid is shown in Figure 5. Increasing the length of the CNTs tends to decelerate the flow in the core region, as shown by the decrease in the streamfunction values (Figure 5b) and vertical velocity (Figure 5c). As a consequence, the temperature of the bio-nanofluid in the core region tends to increase for larger CNTs, as illustrated in Figure 5a, leading to a relatively small decrease of Nu_{av} (Figure 5d).

Another way to control the heat transfer and fluid flow in the porous tumor is by varying the interfacial nanolayer thickness, t. Increasing t leads to relatively higher temperatures in the tumorous region (Figure 6a) due to the decrease in the flow in the core region and in the vertical velocity (Figure 6b,c). This is a consequence of the effective thermal conductivity dependence on nanolayer thickness, shown in Figure 2d; increasing t increases k_{bio} , which leads to a decrease in the Rayleigh number. Thus, the convective heat transfer mode in the tumorous region is less dominant, as also illustrated via the average Nusselt number plot in Figure 6d.

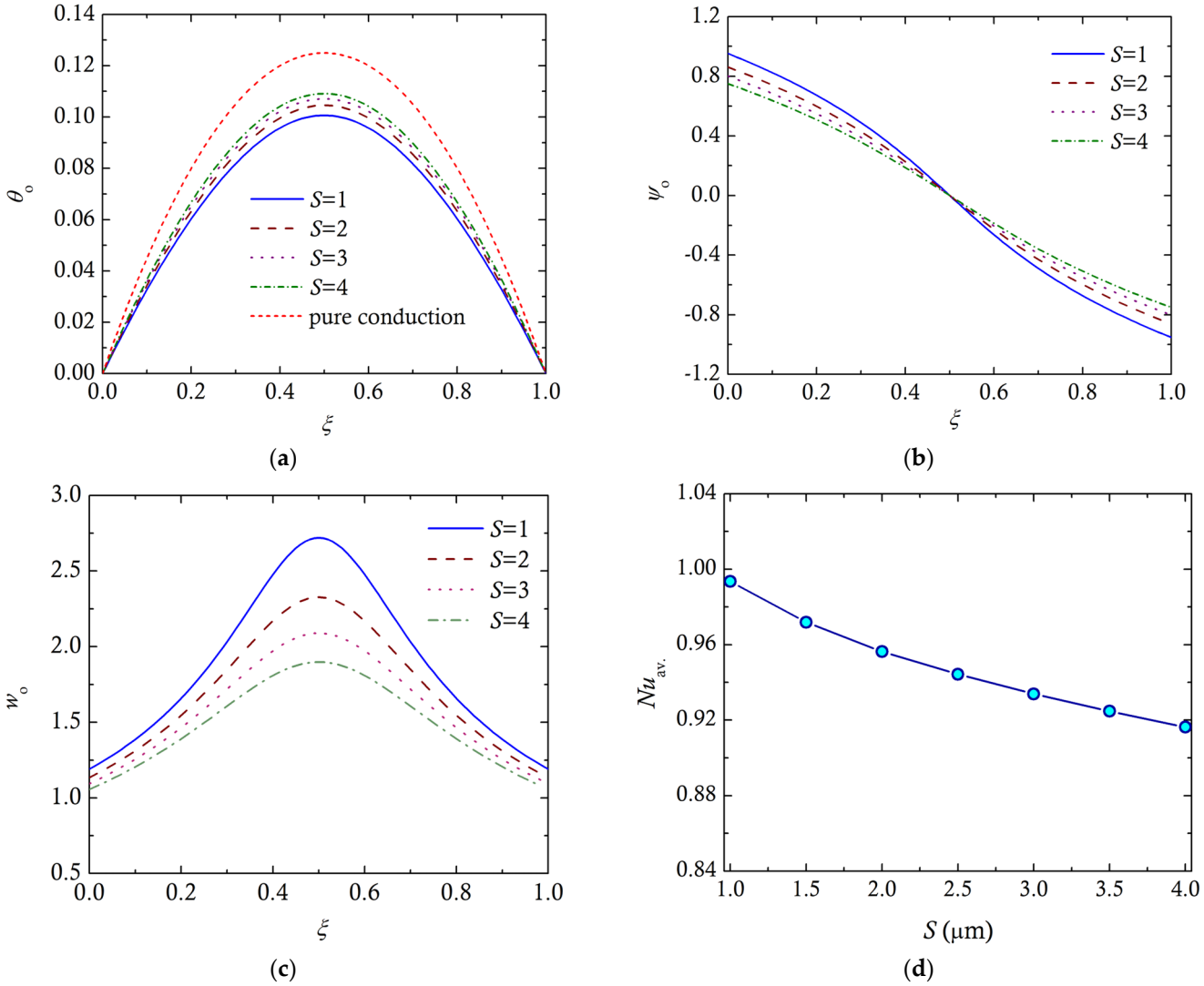


Figure 5. Results for different CNT length (S) in the core region: (**a**) dimensionless temperature profile, $\theta_{0.}$, (**b**) streamfunction, ψ_0, (**c**) dimensionless vertical velocity, w_o, and (**d**) average Nusselt number $Nu_{av.}$.

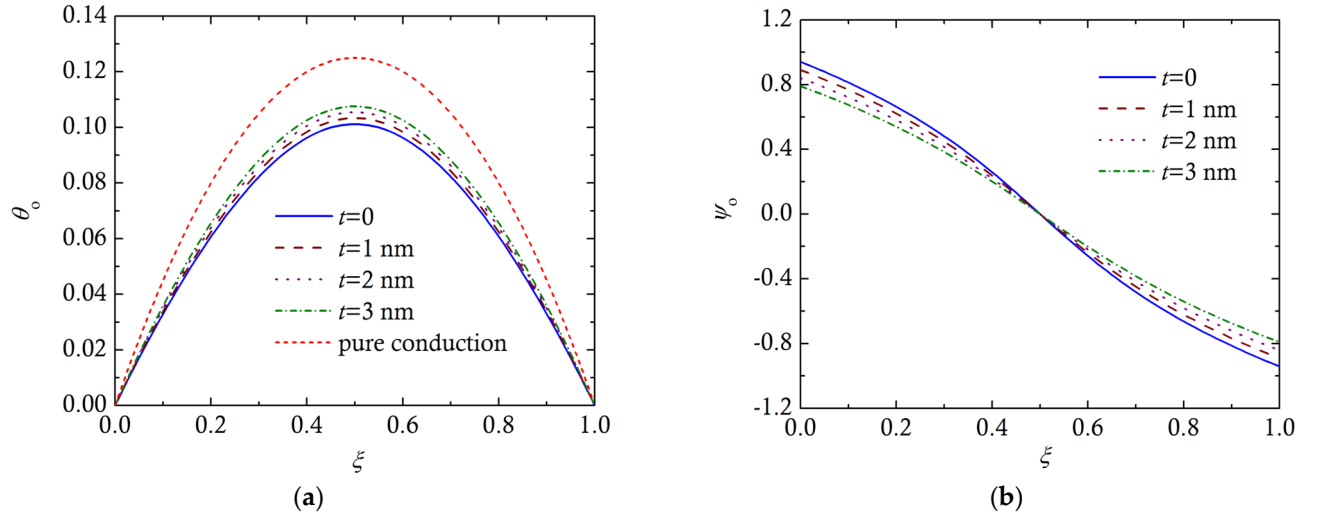


Figure 6. *Cont.*

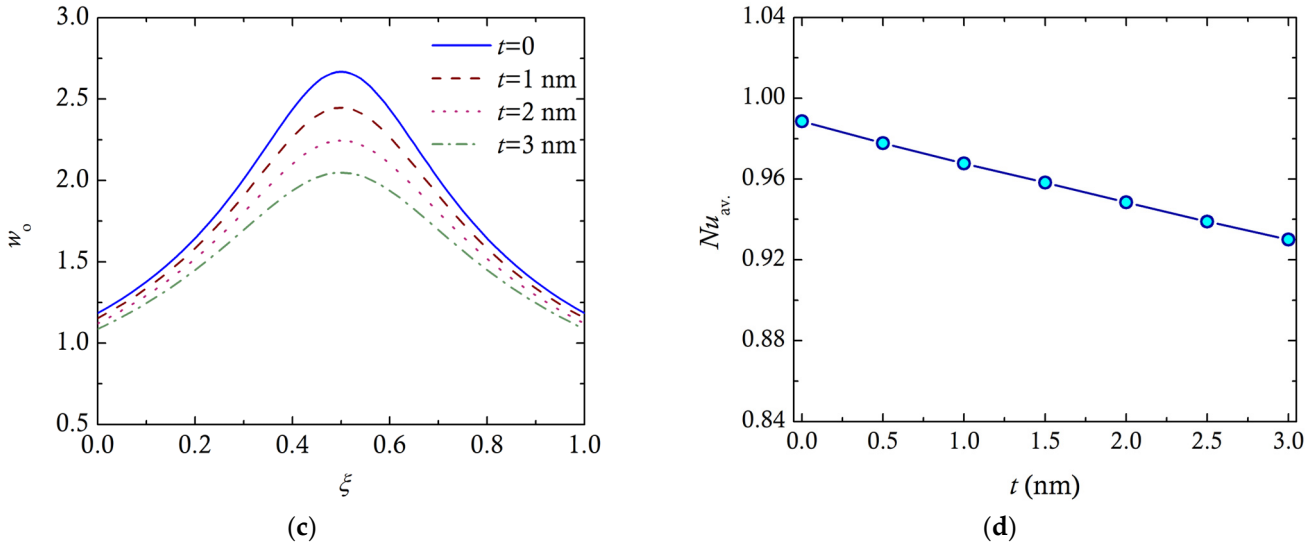


Figure 6. Results for different CNT interfacial nanolayer thickness (t) values in the core region: (**a**) dimensionless temperature profile, $\theta_{0.}$, (**b**) streamfunction, ψ_0, (**c**) dimensionless vertical velocity, w_o, and (**d**) average Nusselt number $Nu_{av.}$.

Figure 7a shows the effect of the CNT volume fraction, φ, on the analytical temperature θ_o. Increasing φ in the tumor leads to a substantial increase in the effective thermal conductivity (see Figure 2e). As a result, Rs_{bio} decreases, which means that heat transfer in the tumor deteriorates, resulting in poor buoyancy flow currents that lead to high temperature values in the core region (Figure 7a). By the same rationale, the velocities and the streamfunction in Figure 7b,c also exhibit a decrease, which means that the bio-nanofluid flow is gradually decelerated as the concentration of the CNTs increases. Figure 7d shows that the $Nu_{av.}$ is remarkably reduced by increasing the volume fraction of the CNTs. In essence, the value of Nu_{av} decreases from approximately 1.14 to 0.84, corresponding to a 26.32% decrease, as φ increases from 0 to 0.04.

It is also important to show how the two dimensionless numbers, Ha and Da affect the heat transfer in the tumor. The effect of the Ha number on Nu_{av} is shown in Figure 8. The increasing Ha results in the substantial decrease of the $Nu_{av.}$ number. At low Ha numbers, the reduction is very steep, and after $Ha \approx 20$ the $Nu_{av.}$ levels-off to the value of about 0.8, which corresponds to pure conduction. The above behavior is attributed to the fact that increasing Ha the flow is slowed down leading to deterioration of heat transfer by convection.

For sufficiently large Ha values, the main mode of heat transfer is essentially conduction. In essence, the value of Nu_{av} decreases from approximately 0.94 to 0.8, corresponding to a 14.89% decrease, as Ha increases from 0 (corresponding to the hydrodynamic limit where no magnetic field is applied) to 50.

Finally, the aim of Figure 9 is to illustrate the effect of the tumor permeability (via the Darcy number, Da) in heat transfer. We have selected to exhibit this behavior for various γ parameter values. At very small Darcy numbers ($Da < 10^{-3}$), the average Nusselt number is relatively uniform across different γ values, implying that the influence of geometry is less significant in this conduction-dominated regime. In the intermediate range ($10^{-3} < Da < 1$) a steep increase in Nu_{av} takes place, and the impact of γ becomes more pronounced. At a large Da($Da > 1$), Nu_{av} stabilizes, with lower γ values leading to enhanced heat transfer. The above picture is reasonable, since more open space in the tumor suggests an increased permeability, which means a decreased flow resistance. Therefore, the bio-nanofluid in the tumor is accelerated, and convective heat transfer is favored.

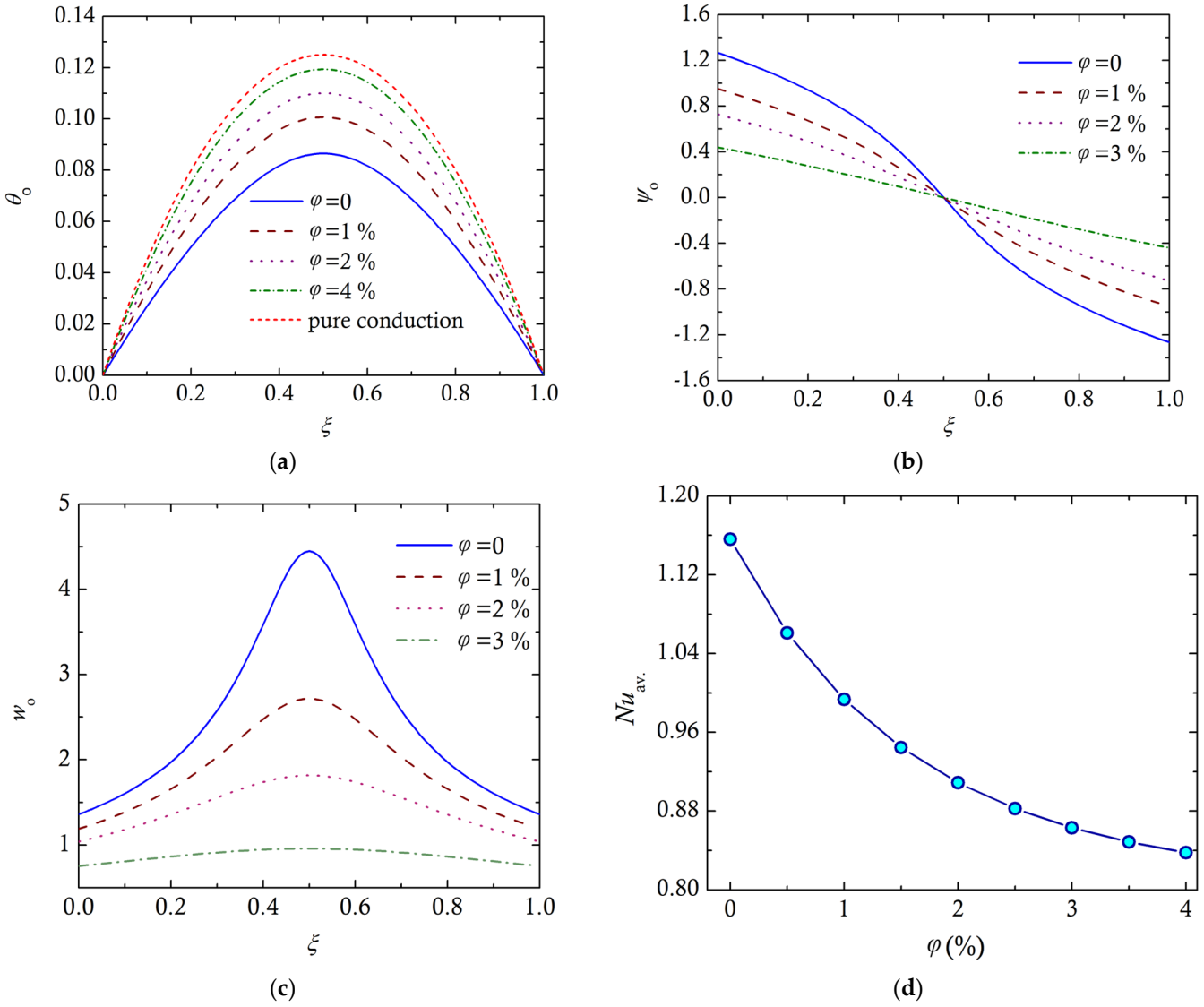


Figure 7. Results for different CNT volume fraction φ values in the core region: (**a**) dimensionless temperature profile, $\theta_{0.}$, (**b**) streamfunction, $\psi_{0.}$, (**c**) dimensionless vertical velocity, w_o, and (**d**) average Nusselt number $Nu_{av.}$.

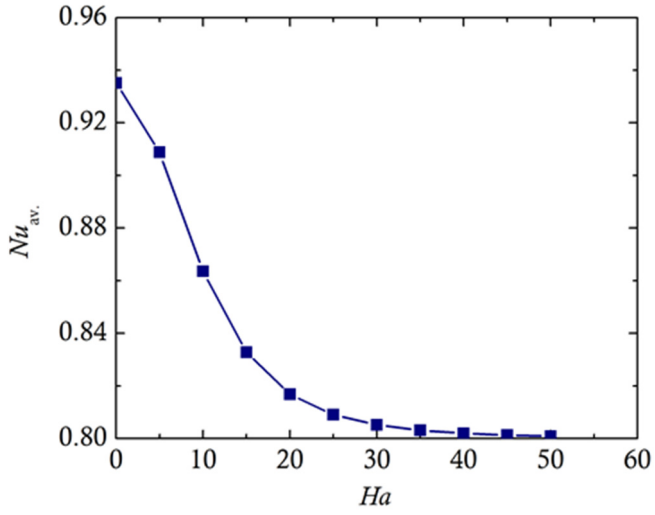


Figure 8. Dependence of average Nusselt number Nu_{av} on the Hartmann number Ha.

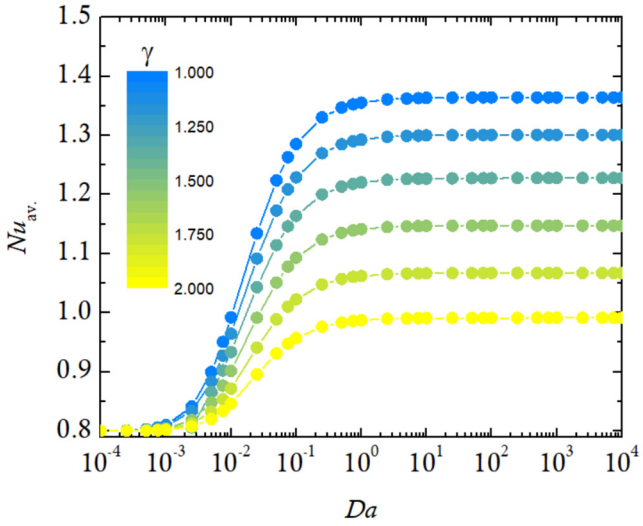


Figure 9. Dependence of average Nusselt number $Nu_{av.}$ on the Darcy number Da for different values of the γ parameter.

Continuing, it should be mentioned that this study examines MHD natural convection within a bio-nanofluid-saturated porous cavity, specifically blood, with CNTs. It extends previous works, such as [26,31], which analyzed nanoparticles in a non-porous medium, and [27], which considered nanoparticles in a porous medium, adapting them to bio-nanofluids. Unlike [16], which used iron oxides, this analysis investigates CNTs to explore their potential for hyperthermia treatment. Consistently with prior findings, an increase in the Hartmann number, due to a higher nanoparticle concentration or stronger magnetic fields, slows nanofluid flow and reduces heat transfer. Similarly, increasing the Rayleigh number, resulting from a lower nanoparticle concentration or higher volumetric heating, enhances fluid motion and heat transfer. Notably, this analysis also revealed how CNT geometric properties influence bio-nanofluid flow and heat transfer, offering valuable insights from a medical engineering perspective for the first time, to the best of the authors' knowledge.

4. Discussion

Hyperthermia of porous tumors using CNTs is a very important treatment to selectively kill cancerous regions via localized heating. In the present study, we have provided a fundamental understanding on how CNTs can be used to control the heat transfer and fluid flow of the bio-nanofluid within the tumor. We elucidated that several geometrical factors related to the molecular structure of CNTs, as well as the volume fraction of the nanoparticles, have a definite impact on heat transfer and fluid flow of the bio-nanofluid in the porous tumor. Consequently, controlling the CNTs shape (i.e., length, diameter, nanolayer thickness) can be used to optimize or provide more control of the hyperthermic effect in the tumor. While our main study focused on CNTs with a cylindrical shape, we have examined some scenarios considering what would happen if the CNT geometry deviated from this shape (through examining different γ values). For example, the study by Choi et al. [41] presents a method to fabricate fully flattened CNTs, while the study by Zeinalipour-Yadzi and Loizidou [42] proposed CNTs with several cap structures at the ends of the CNTs, reminiscent of prolate spheroid shapes. Also, Adorinni et al. [43] and Tripathi et al. [44] reported shapes of carbon nanotropes, like carbon nano-onions and carbon nanohorns, with a high resemblance to oblate spheres and cones. In fact, the study by Tripathi et al. [44] is placed within a drug delivery framework, towards a deeper understanding of human diseases including cancer, genetic disorders and neurodegenerative diseases amongst other.

Therefore, fabricating CNTs with several structures reminiscent of the ones reported above, and taking into account the nanolayer thickness and volume fraction, may pave a new way towards optimizing and tailoring the hyperthermic effect in a patient-wise manner.

The strong dependence of the average Nusselt number on the Hartmann number (Ha_{bio}), as demonstrated in the Results section, provides a mechanism for the precise control of heat transfer and flow during hyperthermia treatment. Analogous to the CZ crystal growth method [30], where magnetic fields are used to improve crystal quality, the MHD effect on bio-nanofluid flow, within porous cancerous tissue, can be leveraged for optimal treatment outcomes. Notably, Ha_{bio} can be regulated not only by adjusting the magnetic field strength (B_0), but also by modifying the CNT volume fraction (φ). This is because the viscosity, density, and electrical conductivity of the bio-nanofluid are influenced by the CNT volume fraction (Equations (12), (13) and (16)). This approach is innovative, because it combines the effects of magnetic fields and CNT volume fraction to precisely control the flow and heat transfer of bio-nanofluids in cancerous tissue. Thus, it offers a new level of control over the treatment process, allowing for a more efficient and personalized cancer therapy, potentially improving outcomes while minimizing side effects.

It should also be mentioned that the nature of the tumor, such as porosity or permeability and shape, also plays an important role for an effective treatment design. For example, during tumor growth, porosity may decrease in early stages, but can increase in later stages due to necrosis or matrix degradation. This is reflected in our study via the Darcy number and the behavior we presented in Figure 8. As a consequence, for different tumor porosities one may regulate the CNTs shape towards enhanced or optimized magnetic hyperthermia treatment results.

Future research could expand upon this work by investigating the effects of dynamic blood-CNT nanofluid flow and pulsatile motion [45,46] within the vasculature on CNT-mediated heat transfer in hyperthermia treatment. Furthermore, the permeability or porosity of the tumor may be non-homogeneous [47,48] and this could be incorporated in the present model. Tumor geometries, like ellipse-like [14] or fractals [49], may be a more realistic description of the tumor shape. The integration of patient-specific tumor geometries obtained from imaging techniques, such as MRI or CT scans, could refine the model to better capture the heterogeneous and anisotropic nature of the tumor environments. Finally, future research should focus on conducting preclinical and clinical trials to evaluate the safety, efficacy, and biocompatibility of bio-nanofluids in human patients. The results from these trials would be essential for refining the treatment methods, ensuring that the therapy is both effective and safe for human use, and ultimately bringing the proposed innovative approach closer to a widespread clinical application.

5. Conclusions

The present study provides a comprehensive analysis of how the geometrical properties of CNTs influence the bio-nanofluid flow and heat transfer in a porous tumor. Key findings reveal that variations in CNT geometry, including diameter, length, interfacial nanolayer thickness, and level of elongation significantly affect the bio-nanofluid flow and heat transfer. Smaller CNT diameters enhance the convective heat transfer by increasing the Rayleigh number, while larger lengths suppress the fluid motion, favoring conduction-dominated heat transfer. Moreover, increasing the interfacial nanolayer thickness (by functionalizing the surface of CNTs with different chemical groups [26]), CNT elongation, and volume fraction, were found to reduce the convective heat transfer by increasing effective thermal conductivity, leading to a reduced buoyancy-driven flow and higher core temperatures. Furthermore, the Darcy number plays a pivotal role, with higher values promoting convective heat transfer due to an increased tumor permeability. These results

highlight the potential for tailoring CNT properties to optimize heat transfer and fluid dynamics in tumor hyperthermia applications, offering valuable insights into biomedical engineering and therapeutic design.

Author Contributions: Conceptualization, N.D.P., E.K., L.B., T.D.P. and I.S.; methodology, N.D.P., E.K. and L.B.; validation, E.K. and L.B.; visualization, E.K. and L.B.; writing—original draft preparation, N.D.P.; writing—review and editing, N.D.P., E.K., T.D.P. and L.B.; supervision, T.D.P. and I.S. All authors have read and agreed to the published version of the manuscript.

Funding: This research received no external funding.

Data Availability Statement: The original contributions presented in this study are included in the article. Further inquiries can be directed to the corresponding author(s).

Conflicts of Interest: The authors declare no conflicts of interest.

References

1. Bray, F.B.; Ferlay, J.; Soerjomataram, I.; Siegel, R.L.; Torre, L.A.; Jemal, A. Global cancer statistics 2018: GLOBOCAN estimates of incidence and mortality worldwide for 36 cancers in 185 countries. *CA A Cancer J. Clin.* **2018**, *68*, 394–424. [CrossRef] [PubMed]
2. Kris, M.G.; Johnson, B.E.; Berry, L.D.; Kwiatkowski, D.J.; Iafrate, A.J.; Wistuba, I.I.; Varella-Garcia, M.; Franklin, W.A.; Aronson, S.L.; Su, P.-F.; et al. Using Multiplexed Assays of Oncogenic Drivers in Lung Cancers to Select Targeted Drugs. *JAMA* **2014**, *311*, 1998–2006. [CrossRef]
3. Perou, C.M.; Sørlie, T.; Eisen, M.B.; van de Rijn, M.; Jeffrey, S.S.; Rees, C.A.; Pollack, J.R.; Ross, D.T.; Johnsen, H.; Akslen, L.A.; et al. Molecular Portraits of Human Breast Tumours. *Nature* **2000**, *406*, 747–752. [CrossRef] [PubMed]
4. Holland, E.C. Glioblastoma multiforme: The terminator. *Proc. Natl. Acad. Sci. USA* **2000**, *97*, 6242–6244. [CrossRef] [PubMed]
5. Gkountas, A.A.; Polychronopoulos, N.D.; Sofiadis, G.N.; Karvelas, E.G.; Spyrou, L.A.; Sarris, I.E. Simulation of magnetic nanoparticles crossing through a simplified blood-brain barrier model for Glioblastoma multiforme treatment. *Comput. Methods Programs Biomed.* **2021**, *212*, 106477. [CrossRef]
6. Dagogo-Jack, I.; Shaw, A.T. Tumour heterogneeity and resistance to cancer therapies. *Nat. Rev. Clin. Oncol.* **2018**, *15*, 81–94. [CrossRef]
7. Senapati, S.; Mahanta, A.K.; Kumar, S.; Maiti, P. Controlled drug delivery vehicles for cancer treatment and their performance. *Signal Transduct. Target. Ther.* **2018**, *3*, 7. [CrossRef]
8. Verma, J.; Lal, S.; Van Noorden, C.J.F. Nanoparticles for hyperthermic therapy: Synthesis strategies and applications in glioblastoma. *Int. J. Nanomed.* **2014**, *9*, 2863–2877.
9. Zhang, Y.; Calderwood, S.K. Autophagy, protein aggregation and hyperthermia: A mini-review. *Int. J. Hyperth.* **2011**, *27*, 409–414. [CrossRef]
10. De Pasquale, D.; Pucci, C.; Desii, A.; Marino, A.; Debellis, D.; Leoncino, L.; Prato, M.; Moscato, S.; Amadio, S.; Fiaschi, P.; et al. A Novel Patient-Personalized Nanovector Based on Homotypic Recognition and Magnetic Hyperthermia for an Efficient Treatment of Glioblastoma Multiforme. *Adv. Healthc. Mater.* **2023**, *12*, 2203120. [CrossRef]
11. Tehrani, M.H.H.; Kashkooli, F.M.; Soltani, M. Effect of tumor heterogeneity on enhancing drug delivery to vascularized tumors using thermo-sensitive liposomes triggered by hyperthermia: A multi-scale and multi-physics computational model. *Comput. Biol. Med.* **2024**, *170*, 108050. [CrossRef]
12. Khandhar, A.P.; Ferguson, R.M.; Simon, J.A.; Krishnan, K.M. Enhancing cancer therapeutics using size-optimized magnetic fluidhyperthermia. *J. Appl. Phys.* **2012**, *111*, 7B306. [CrossRef] [PubMed]
13. Chicheł, A.; Skowronek, J.; Kubaszewska, M.; Kanilowski, M. Hyperthermia—Description of a method and a review of clinical applications. *Rep. Pract. Oncol. Radiother.* **2007**, *12*, 267–275. [CrossRef]
14. Polychronopoulos, N.D.; Gkountas, A.A.; Sarris, I.E.; Spyrou, L.A. A computational study on magnetic nanoparticles hyperthermia of ellipsoidal tumors. *Appl. Sci.* **2021**, *11*, 9526. [CrossRef]
15. DeNardo, G.L.; DeNardo, S.J. Turning heat on cancer. *Cancer Biother. Radiopharm.* **2018**, *23*, 671–680.
16. Benos, L.; Ninos, G.; Polychronopoulos, N.D.; Exomanidou, M.A.; Sarris, I. Natural Convection of Blood–Magnetic Iron Oxide Bio-nanofluid in the Context of Hyperthermia Treatment. *Computation* **2022**, *10*, 190. [CrossRef]
17. Hauck, T.S.; Jennings, T.L.; Yatsenko, T.; Kumaradas, J.C.; Chan, W.C.W. Enhancing the Toxicity of Cancer Chemotherapeutics with Gold Nanorod Hyperthermia. *Adv. Mater.* **2008**, *20*, 3832–3838. [CrossRef]
18. Naderi, N.; Lalebeigi, F.; Sadat, Z.; Eivazzadeh-Keihan, R.; Maleki, A.; Mahdavi, M. Recent advances on hyperthermia therapy applications of carbon-based nanocomposites. *Colloids Surf. B. Biointerfaces* **2023**, *228*, 113430. [CrossRef]

19. Burke, P.J.; Li, S.D.; Yu, Z. Quantitative theory of nanowire and nanotube antenna performance. *IEEE Trans. Nanotechnol.* **2006**, *5*, 314–334. [CrossRef]
20. Zhou, G.; Duan, W.; Gu, B. First-principles study on morphology and mechanical properties of single-walled carbon nanotube. *Chem. Phys. Lett.* **2001**, *333*, 344–349. [CrossRef]
21. Glazer, E.S.; Curley, S.A. Non-invasive radiofrequency ablation of malignancies mediated by quantum dots, gold nanoparticles and carbon nanotubes. *Ther. Deliv.* **2011**, *2*, 1325–1330. [CrossRef] [PubMed]
22. Markovic, Z.M.; Harhaji-Trajkovic, L.M.; Todorovic-Markovic, B.M.; Kepić, D.P.; Arsikin, K.M.; Jovanović, S.P.; Pantovic, A.C.; Dramićanin, M.D.; Trajkovic, V.S. In vitro comparison of the photothermal anticancer activity of graphene nanoparticles and carbon nanotubes. *Biomaterials* **2011**, *32*, 1121–1129. [CrossRef] [PubMed]
23. Raniszewski, G.; Miaskowski, A.; Wiak, S. The application of carbon nanotubes in magnetic fluid hyperthermia. *J. Nanomater.* **2015**, *2015*, 527652. [CrossRef]
24. Radzi, M.R.M.; Johari, N.A.; Zawawi, W.F.A.W.W.M.; Zawawi, N.A.; Latiff, N.A.; Malek, N.A.N.N.; Wahab, A.A.; Salim, M.I.; Jemon, K. In vivo evaluation of oxidized multiwalled-carbon nanotubes-mediated hyperthermia treatment for breast cancer. *Biomater. Adv.* **2022**, *143*, 112586. [CrossRef]
25. Mahjoob, S.; Vafai, K. Analytical characterization of heat transport through biological media incorporating hyperthermia treatment. *Int. J. Heat Mass Transf.* **2009**, *52*, 1608–1618. [CrossRef]
26. Benos, L.T.; Karvelas, E.G.; Sarris, I.E. A theoretical model for the magnetohydrodynamic natural convection of a CNT-water nanofluid incorporating a renovated Hamilton-Crosser model. *Int. J. Heat Mass Transf.* **2019**, *135*, 548–560. [CrossRef]
27. Benos, L.T.; Polychronopoulos, N.D.; Mahabaleshwar, U.S.; Lorenzini, G.; Sarris, I.E. Thermal and flow investigation of MHD natural convection in a nanofluid-saturated porous enclosure: An asymptotic analysis. *J. Therm. Anal. Calorim.* **2021**, *143*, 751–765. [CrossRef]
28. Bain, B.J. *Blood Cells: A Practical Guide*, 6th ed.; Wiley: Hoboken, NJ, USA, 2022.
29. Benos, L.; Spyrou, L.A.; Sarris, I.E. Development of a new theoretical model for blood-CNTs effective thermal conductivity pertaining to hyperthermia therapy of glioblastoma multiform. *Comput. Methods Programs Biomed.* **2019**, *172*, 79–85. [CrossRef]
30. Zhang, N.; Liu, D. Numerical simulation of MHD oscillatory mixed convection in CZ crystal growth by Lattice Boltzmann method. *Results Phys.* **2018**, *10*, 882–890. [CrossRef]
31. Benos, L.T.; Kakarantzas, S.C.; Sarris, I.E.; Grecos, A.P.; Vlachos, N.S. Analytical and numerical study of MHD natural convection in a horizontal shallow cavity with heat generation. *Int. J. Heat Mass Transf.* **2014**, *75*, 19–30. [CrossRef]
32. Jiang, H.; Xu, Q.; Huang, C.; Shi, L. The role of interfacial nanolayer in the enhanced thermal conductivity of carbon nanotube-based nanofluids. *Appl. Phys. A* **2015**, *118*, 197–205. [CrossRef]
33. Baskurt, O.K.; Meiselman, H.J. Blood rheology and hemodynamics. *Semin. Thromb. Hemost.* **2003**, *29*, 435–450. [CrossRef] [PubMed]
34. Nader, E.; Skinner, S.; Romana, M.; Fort, R.; Lemonne, N.; Guillot, N.; Gauthier, A.; Antoine-Jonville, S.; Renoux, C.; Hardy-Dessources, M.-D.; et al. Blood Rheology: Key Parameters, Impact on Blood Flow, Role in Sickle Cell Disease and Effects of Exercise. *Front. Physiol.* **2019**, *10*, 1329. [CrossRef] [PubMed]
35. Abu-Libdeh, N.; Redouane, F.; Aissa, A.; Mebarek-Oudina, F.; Almuhtady, A.; Jamshed, W.; Al-Kouz, W. Hydrothermal and Entropy Investigation of Ag/MgO/H2O Hybrid Nanofluid Natural Convection in a Novel Shape of Porous Cavity. *Appl. Sci.* **2021**, *11*, 1722. [CrossRef]
36. Al-Farhany, K.; Al-Chlaihawi, K.K.; Al-dawody, M.F.; Biswas, N.; Chamkha, A.J. Effects of fins on magnetohydrodynamic conjugate natural convection in a nanofluid-saturated porous inclined enclosure. *Int. Commun. Heat Mass Transf.* **2021**, *126*, 105413. [CrossRef]
37. Al-Rashed, A.A.A.; Kolsi, L.; Öztop, H.F.; Aydi, A.; Malekshah, E.H.; Abu-Hamdeh, N.; Borjini, M.N. 3D magneto-convective heat transfer in CNT-nanofluid filled cavity underpartially active magnetic field. *Physica E* **2018**, *99*, 294–303. [CrossRef]
38. Kolsi, L.; Al-Rashed, A.A.A.; Al-Salem, K.; Öztop, H.F.; Borjini, M.N. Control of natural convection via inclined plate of CNT-water nanofluid in an open sided cubical enclosure under magnetic field. *Int. J. Heat Mass Transf.* **2017**, *111*, 1007–1018. [CrossRef]
39. Job, V.M.; Gunakala, S.R. Unsteady MHD free convection nanofluid flows within a wavy trapezoidal enclosure with viscous and Joule dissipation effects. *Numer. Heat Transf. Part A.* **2016**, *69*, 421–443. [CrossRef]
40. Daniels, P.; Jones, O. Convection in a shallow cavity due to internal heat generation. *Int. J. Heat Mass Transf.* **1998**, *41*, 3979–3987. [CrossRef]
41. Choi, D.H.; Wang, Q.; Azuma, Y.; Majima, Y.; Warner, J.H.; Miyata, Y.; Shinohara, H.; Kitaura, R. Fabrication and characterization of fully flattened carbon nanotubes: A new graphene nanoribbon analogue. *Sci. Rep.* **2013**, *3*, 1617. [CrossRef]
42. Zeinalipour-Yazdi, C.D.; Loizidou, E.Z. Study of the cap structure of (3,3), (4,4) and (5,5)-SWCNTs: Application of the sphere-in-contact model. *Carbon* **2017**, *115*, 819–827. [CrossRef]
43. Adorinni, S.; Cringoli, M.C.; Perathoner, S.; Fornasiero, P.; Marchesan, S. Green approaches to carbon nanostructure-based biomaterials. *Appl. Sci.* **2021**, *11*, 2490. [CrossRef]

44. Tripathi, A.C.; Saraf, S.A.; Saraf, S.K. Carbon nanotropes: A contemporary paradigm in drug delivery. *Materials* **2015**, *8*, 3068–3100. [CrossRef]
45. Dawood, A.S.; Kroush, F.A.; Abumandour, R.M.; Eldesoky, I.M. Pulsatile nanofluid flow with variable pressure gradient and heat transfer in wavy channel. *Sci. Rep.* **2024**, *14*, 9351. [CrossRef]
46. Najafi, N.; Almosawy, W.; Abbas, M.S.; Goligerdian, A.; Najafi, M.; Abdi, N.; Ardalan, A.; Aminian, S. Comparative analysis of the silver gold and copper-titanium dioxide hybrid nanoparticles impact on flow and heat transfer of the pulsatile blood in occluded cerebral artery. *J. Therm. Biol.* **2025**, *127*, 104060. [CrossRef]
47. Pereira, R.C.; Santagiuliana, R.; Ceseracciu, L.; Boso, D.P.; Schrefler, B.A.; Decuzzi, P. Elucidating the role of matrix porosity and rigidity in glioblastoma type IV progression. *Appl. Sci.* **2020**, *10*, 9076. [CrossRef]
48. Andreozzi, A.; Brunese, L.; Iasiello, M.; Tucci, C.; Vanoli, G.P. Numerical investigation of a thermal ablation porous media-based model for tumoral tissue with variable porosity. *Computation* **2021**, *9*, 50. [CrossRef]
49. Lennon, F.; Cianci, G.; Cipriani, N.; Hensing, T.A.; Zhang, H.J.; Chen, C.T.; Murgu, S.D.; Vokes, E.E.; Vannier, M.W.; Salgia, R. Lung cancer—A fractal viewpoint. *Nat. Rev. Clin. Oncol.* **2015**, *12*, 664–675. [CrossRef]

Disclaimer/Publisher's Note: The statements, opinions and data contained in all publications are solely those of the individual author(s) and contributor(s) and not of MDPI and/or the editor(s). MDPI and/or the editor(s) disclaim responsibility for any injury to people or property resulting from any ideas, methods, instructions or products referred to in the content.